Phased-Array Doppler Sonar measurements of near-surface motion: Langmuir circulation, surface waves, and breaking.

Jerome A. Smith,[1]

[1]Scripps Intitution of Oceanography, La Jolla CA 92093, USA. jasmith@ucsd.edu

Abstract

Movies of surface currents from "Phased-Array Doppler Sonars" (PADS) have helped to elucidate several phenomena. In the open ocean, velocity scales for Langmuir circulation were examined relative to wind and waves. Near shore, a dual-PADS arrangement produced horizontal velocity vectors over a 300 m by 400 m area, monitoring waves and currents for weeks. Recently, a system was aimed up at a "vertical slice" of the motion under a breaking wave crest, revealing interesting bubble and velocity structures.

1. Introduction

Over the past decade, measurements have been made in a variety of places using "Phased-Array Doppler Sonars" (PADS). The approach is to use high-frequency acoustic "repeat-sequence codes" [1-3] to estimate radial velocities as a function of range and angle from each of the PADS. The signal is emitted in a wide horizontal fan. Some backscattered sound returns to the sonar, where the signal is received on a 16 element array and analyzed for frequency shift versus angle and elapsed time since transmission. The frequency shift of the backscattered signal is proportional to the radial component of the velocity of the scatterers. The time-delay since transmission translates to distance from the sonar via knowledge of the soundspeed in the water. The vertical direction is unresolved; the effective depth of measurement depends on the vertical distribution of scatterers. Typically, bubbles are the most efficient scatterers, and these tend to be concentrated toward the surface [4]. The resulting time-series of spatial maps (movies) have helped to develop new understandings of the kinematics, scaling, and dynamics of various phenomena.

Here efforts in three distinct areas of research are considered: open ocean mixed layer dynamics (Section 2); nearshore circulation and wave propagation (Section 3); and deep water wave breaking kinematics (Section 4). Section 2 describes how, in the open ocean, the horizontal patterns associated with Langmuir circulation (LC) have been elucidated as storms develop and run their course. In particular, surface velocities associated with LC scale with both wind speed and wave characteristics. Once LC is established, scaling with wave characteristics appears to dominate. However, the scaling factor varies significantly from one wind event to another, indicating further research is needed. Section 3 describes a "dual-Doppler" deployment that was executed in shallow water near shore in 1997, at the Field Research Facility (FRF) of the Army Corps of Engineers, in Duck, NC. With this arrangement, both horizontal velocity components could be estimated over an area some 300 to 400 m on a side. Incident surface waves, edge waves, and the underlying currents were monitored for about 2 months. Section 4 describes a recent deployment (1999) of one of the PADS on the R/P FLIP, looking straight up from 14 m depth at a "slice" of the water just below the ocean surface. It was operated in a ping-to-ping coherent mode, providing about 5 cm by 25 cm resolution and sampling at up to 52 frames per second. Some roughly one meter amplitude waves were occasionally breaking. Both the acoustic intensity (related to bubble density) and the velocities deduced from motion of features (particle image velocimetry) are of interest.

2. Langmuir circulation

Observations of the mixed layer often reveal coherent structures. One such structure consists of horizontal rolls having axes aligned with the wind, named "Langmuir circulation" in honor of the first documentation [5]. This can dominate wind mixing of the surface layer of lakes [5] and oceans [6]. A mechanism for the generation of Langmuir circulation was identified in the late 1970s, based on an interaction between waves and wind-driven currents [7-11]. To investigate the form and dynamics of wind-mixing at the surface of the ocean, observations of wind stress, waves, stratification, velocity profiles, and surface fields of radial velocity and acoustic backscatter intensity were made over several month-long experiments during the past couple decades. In the "Marine Boundary Layer Experiment" (MBLEX), one PADS system was used to image an area of the surface via digital beamforming, sampling the whole area every 0.75 s (see Figure 1). The PADS data were gathered continuously, spanning a storm, so mixed layer evolution was observed over all phases of storm and wave development [12]. To estimate time series of the near-surface velocity scale associated with Langmuir circulation, data averaged over 1 to 3 minutes were employed (filtering out surface waves). Time series of hourly rms velocity for a wind event

during leg-1 of MBLEX are shown in Figure 2. Wind speed W and Stokes' drift U^S are also shown, scaled by constants chosen to yield reasonable fits to the rms velocities over the middle section of the time period. Streaks are first seen sometime after year-day 67.7, as the wind exceeds 8 m/s. It is reasonable to restrict analysis to the segment after this. From there to the end of the segment, the strength scale of surface velocity features follow the surface Stokes' drift due to the waves more closely than they do the wind [13].

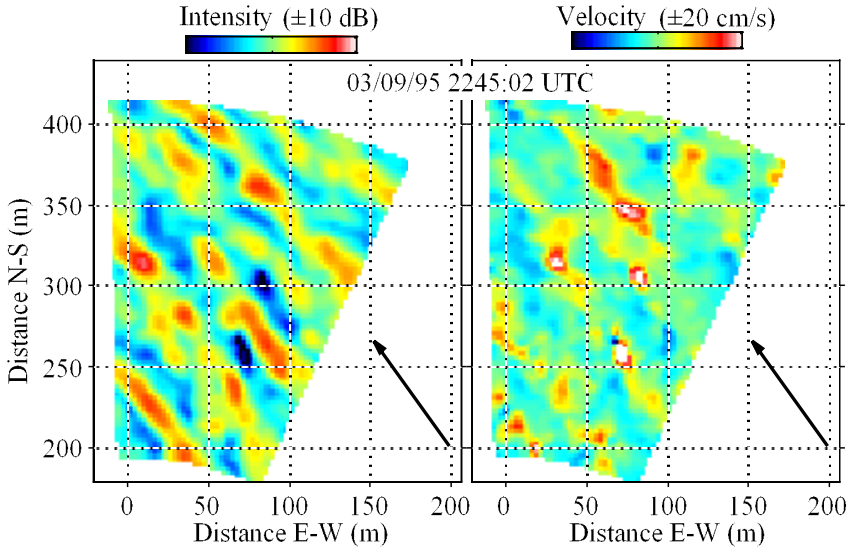

Figure 1. Example frame of PADS data: (Left panel) acoustic backscatter intensity; (right panel) radial velocity. The arrows indicate wind speed (15 m/s) and direction (North is up). The data are smoothed to 3 minute averages, following the mean flow across the area. Contours are relative to the area mean.

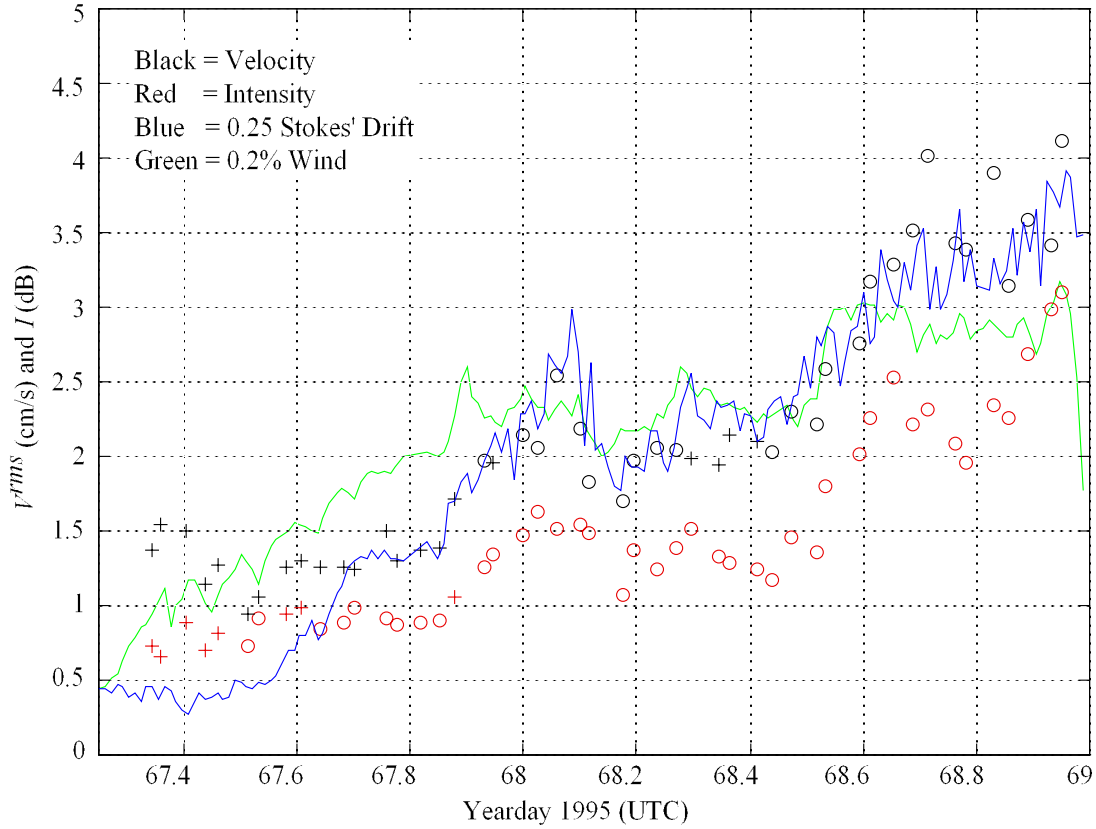

Figure 2. RMS radial velocity (black symbols) and intensity (red symbols) associated with the features, versus time. Each symbol represents a half-hour average; crosses represent dubious estimates, circles more reliable ones. For scaling and comparison, $0.25U^S$ (blue line) and $0.002W$ (green line) are also shown.

3. Near-shore waves and currents

A "dual-Doppler" deployment was executed in shallow water near shore in 1997, at the Field Research Facility of the Army Corps of Engineers, Duck, NC (FRF). With this arrangement, two horizontal velocity components can be estimated over an area some 300 to 400 m on a side (Figure 3). Incident surface waves, edge waves, and the underlying currents were monitored for about 2 months.

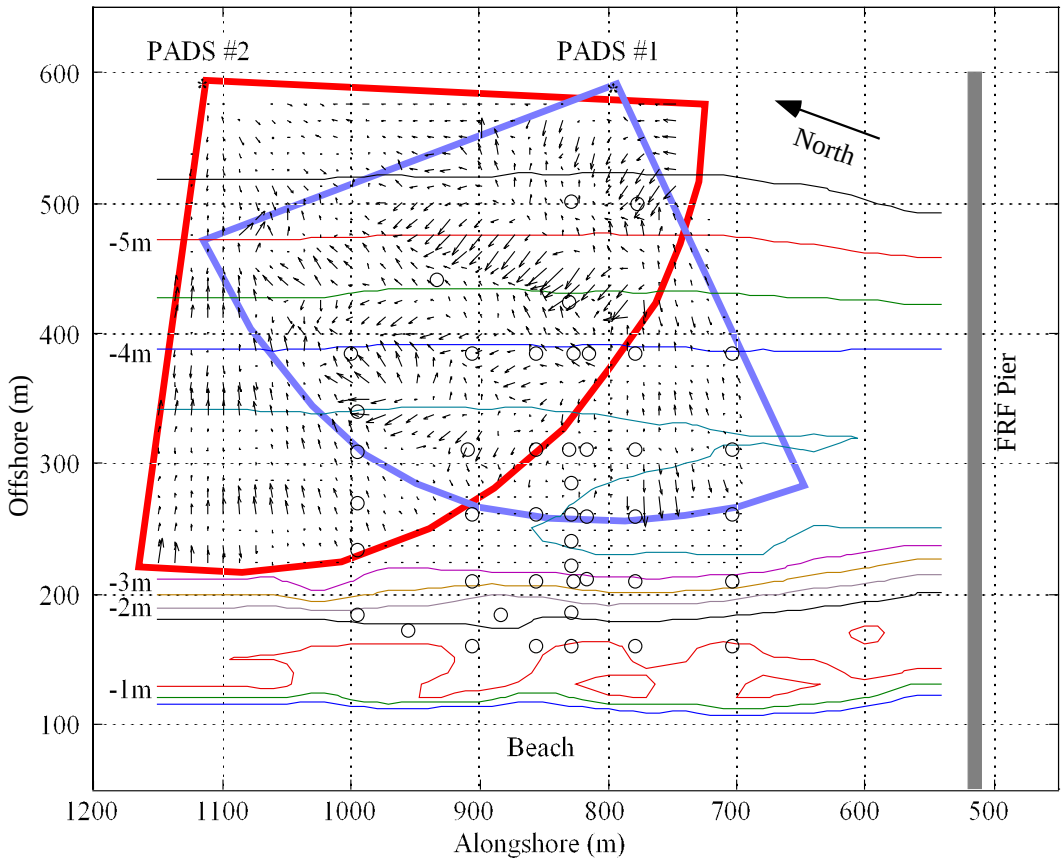

Figure 3. SandyDuck experimental site, showing the area covered by two "Phased Array Doppler Sonars" (PADS). The arrows indicate velocity estimates from a single "snapshot," dominated by swell from the upper right (SE); the longer arrows here correspond to velocities approaching 1 m/s. Both horizontal components are estimated in the overlap region, but only one in the corners covered by a single sonar. The circles show locations of instrumented frames deployed by various collaborating investigators. Depth contours are for the time of the snapshot. Location: Field Research Facility (FRF) of the US Army Corps of Engineers, Duck, North Carolina.

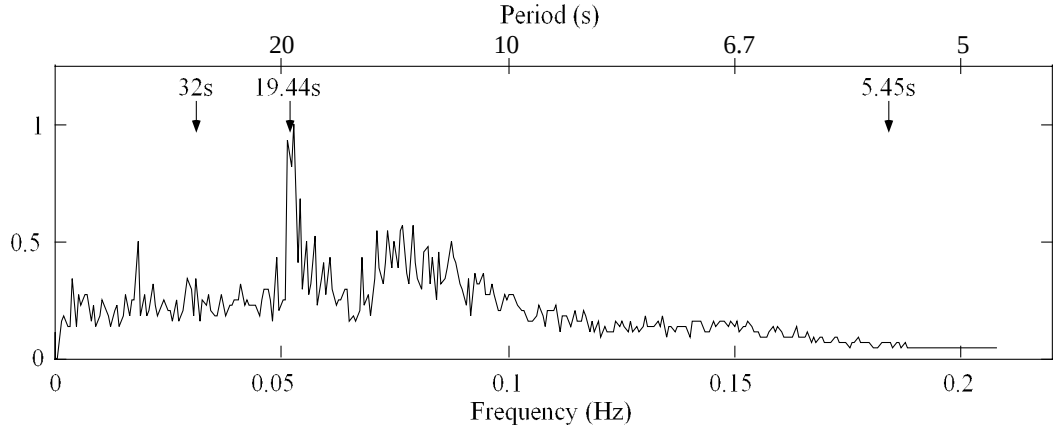

Figure 4. Frequency spectrum of the cross-shore component of velocity (linear, normalized to maximum = 1.0), averaged over the area sampled by the PADS systems (see Figure 3). Note the narrow peak near 0.05 Hz (swell from distant hurricane Erica to the SE) and a broad peak near 0.08 Hz (also swell). Lower but finite spectral levels are seen near 0.15 Hz (local seas) and below 0.05 Hz (the infra-gravity band). Arrows indicate frequencies (periods) at which spatial distributions of variance or wavenumber spectra are considered.

Data for this example were gathered as part of "SandyDuck," a large ONR-sponsored experiment conducted in the fall of 1997 at the Field Research Facility of the Army Corps of Engineers, near Duck NC. The sample area spans a modest depth range (3.5 to 5.5 m depth; see Figure 3). Since surface wave dispersion (for example) depends functionally on depth as the square-root or weaker, significant insight can be gained from the 3D spectra estimated without corrections for these changes in depth. In shallow water there is competition between bottom and volume backscatter, introducing a systematic attenuation of the velocity estimates; however, these variations in response are large-scale and slowly varying with respect to the surface wave field. Thus, while the estimated velocities may be low, the location of nodes and anti-nodes are faithfully reproduced, as are the overall spectral form and peak locations.

Figure 4 shows the 1D frequency spectrum, averaged over the sample area and normalized by the maximum value (significant wave height was about 1.1 m). At the time the data were gathered, winds had just begun to rise from the NE, and the offshore wave field was characterized by two swell systems: from the ESE (19 s period) and SE (12 s period). We first examine the distributions of variance in physical space at two frequencies: (1) 0.031 Hz, where edge-waves and leaky modes dominate; and (2) 0.053 Hz, focusing on long swell incident from the distant hurricane "Erica." Then we shall look at the wavenumber distribution near 0.183 Hz, showing energy near both the free-wave dispersion surface and a bound-wave surface. Complete 3D spectra for this and other example time periods may be viewed as movies, showing the power densities versus wavenumber at one frequency per frame (available on a web-page at http://jerry.ucsd.edu/NSWspectra.html).

The patterns of nodes and anti-nodes revealed in the spatial maps of variance at each frequency provide a compelling tool for the identification of modal structures. For example, spatial maps of variance near 32 s and 19 s periods show distinct nodes and anti-nodes, indicating reflection of these long waves off the beach (Figure 5). The locations of the nodes (as functions of frequency) depend on the bottom topography shoreward of the viewed area. This is true for both incident surf (e.g., for 19 s waves) and for edge-wave (trapped) or leaky modes (e.g., for 32 s periods). There is good reason to hope that nodal and propagation speed information at a variety of frequencies could be "inverted" to deduce the bathymetry and current structure shoreward of the viewed area [14, 15]. This plane-beach case illustrates faithful reproduction of partially reflected waves, including edge-waves. A greater benefit would come in more complex regions, where the modal structure may not be reliably known beforehand; for example in an area where a submarine canyon intersects the shoreline.

In addition to spatial variance maps, the phase structure at each frequency can be plotted, augmenting the understanding of the modal structures. In the simplest cases this would provide propagation speed and direction information. In more complex cases, it could identify amphidromic points, as seen in tidal analyses for ocean basins.

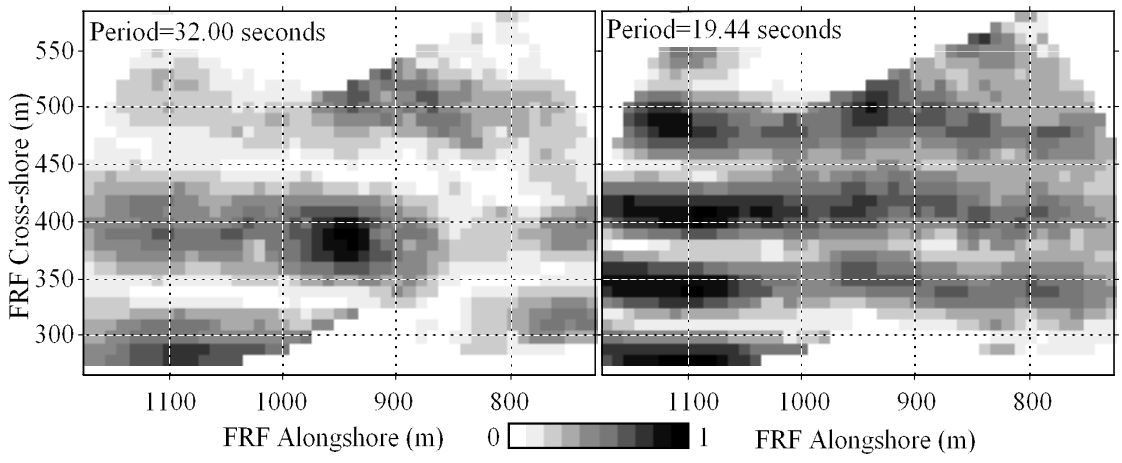

Figure 5. Spatial maps of shore-normal velocity variance at two frequencies: (left) 0.031 Hz (32 s period); (right) 0.053 Hz (19 s period). Each panel is scaled relative to the maximum observed value at the given frequency. Nodes and anti-nodes parallel to shore indicate partial reflection of wave energy. Note that node locations change with frequency, and that the spacing is consistent with shallow-water dispersion as expected for gravity-waves at both frequencies (this would hold true for edge-waves as well as free waves). The patterns may vary weakly in the alongshore direction due to the proximity of the FRF pier (located at x = 520 m).

The three dimensional (2 space and time) views of horizontal velocity sampled by PADS systems invites analysis via 3D Fourier analysis. The full 3D spectrum is unconstrained with respect to dispersion. Figure 6 shows shaded contours of spectral density versus wavenumber at 0.183 Hz, a frequency high enough to

distinguish between finite-depth dispersion and the shallow-water limit. One peak lies along the shallow-water limit, while the other lies along the free-wave dispersion circle. The physical interpretation is that the power density on the shallow-water dispersion circle must be associated with waves bound to lower frequency motions; e.g., harmonics of the 12 and/or 19 second period swell. The directions are consistent with this: the swell are directed from SE to ESE, as is the peak on the inner circle of Figure 6. The other peak, on the free-wave dispersion circle, is consistent with local generation by the NE winds (i.e., propagating toward shore and to the south, in the lower right quadrant of the wavenumber plane.

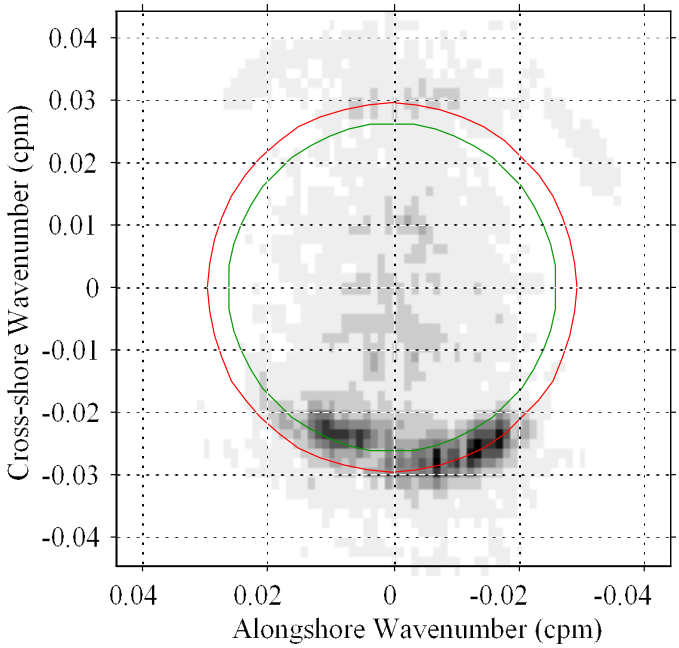

Figure 6. Spectral density versus 2D wavenumber at 0.183 Hz (period 5.45 s), for the shore-normal component of velocity. At this frequency the free-wave dispersion curve (outer circle) is distinguishable from the shallow-water limit (inner circle) by the present measurement technique. Variance lying on the shallow-water limit curve must be associated with harmonics of lower frequency surface waves. The spectral peak centered on the inner circle indicates a propagation direction roughly coincident with the lower frequency peaks. The direction of the free-wave peak is consistent with local winds from the NE (from the upper right to the lower left).

Three-dimensional spectral analysis permits examination of propagation characteristics in detail, without ambiguities concerning propagation direction or the partition of energy between oppositely-directed components. The ability to make this fine a distinction in the dispersion characteristics, and to separate unambiguously a propagating wave from its 180° reflection, appears to be unique among current wave measurement techniques. For example, the second-order generation of double frequency “microseisms” could be directly estimated [16].

Continuous data collection over weeks at a time, as implemented at SandyDuck, captures lower-frequency motions like eddies, fresh-water outflows or surges, and tides as well. At lower frequencies, baroclinicity can be important, emphasizing the need for auxiliary measurements of the vertical structure; e.g., velocity and density profiles at several locations near the sampled area.

4. Cross-section of a breaking wave

One of the greatest challenges in the study of the air-sea interface is presented by breaking waves. Entrainment of gases and the expulsion of droplets and particles by breaking waves are of primary importance to gas fluxes in particular and air/sea exchanges in general. The surface roughness and turbulence near the surface are key to understanding the kinematics and dynamics of this elusive interface. Unfortunately, it is nearly impossible to obtain measurements closer than a meter or two below actively breaking wave crests.

Here, high-resolution ultrasound measurements from an up-looking phased-array system are presented. The system provides digitally beamformed measurements over "pies" about 22 degrees wide by 16 m maximum range, with resolutions of about 1.5 degrees by 5 cm. The instrument was mounted 13.5 m below the mean surface, so the cell size near the surface is about 5 cm (vertical) by 30 cm (along-wind). Sequences of intensity images form a “movie” that can be analyzed for motion as well as for relative scatterer (bubble) density.

Data presented were obtained as a wave of about 2.5 m height crest to trough passed through the field of view

while breaking (one of several breakers captured over a two-week deployment from R/P FLIP). Figure 7 shows a frame from a PADS movie of acoustic intensity, from data taken between 16:24 and 16:25 UTC, 9/16/1999 (9:24 am local time) on the open ocean (~4000 m deep) about 200 km west of San Diego, CA.

By tracking features in time and space over the 2D sample area, the background velocity field can be estimated (Figure 8). One significant feature is the surface. However, by its nature only the vertical velocity can be estimated there. The surface is located in each frame as follows: Beamforming is over-resolved, producing 31 beams from the 16 receivers (the Nyquist wavenumber is not processed). Analysis is restricted to the center 13 beams, ranges 8 to 16 m. Along each beam, the nearest range after the maximum that falls 13 dB below the maximum is identified. The 3 farthest outliers from the median of the 13 values are rejected. A line is fitted to the remaining points, providing the surface location and slope directly above the sonar. Finally, the time series of height and slope are de-spiked (median filtered using 15 points). Dropouts introduced by dense bubble clouds are an issue, and this procedure was developed to minimize the effect.

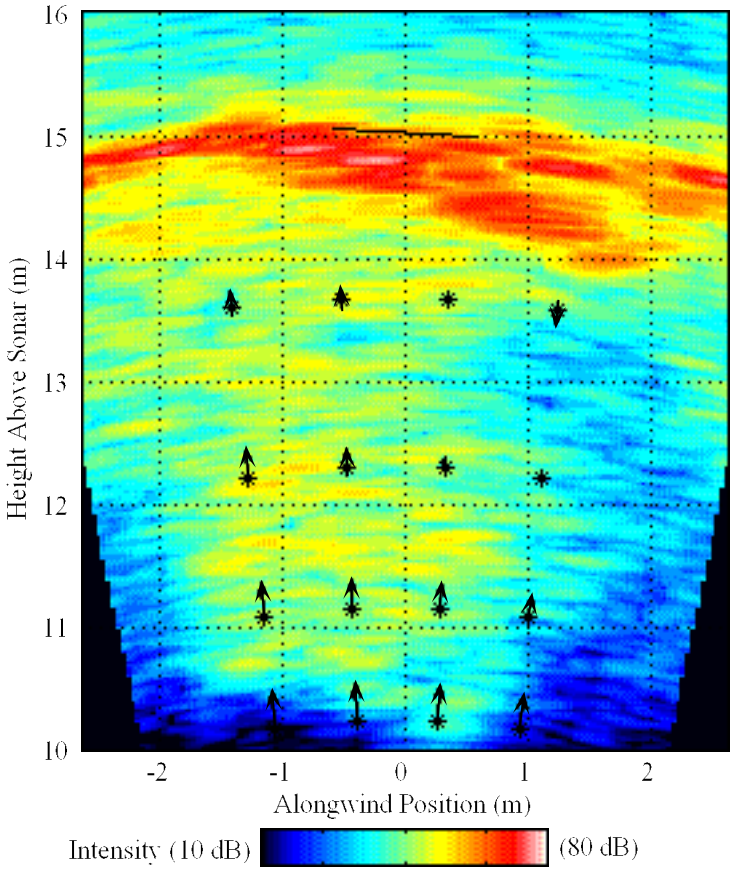

Figure 7. One frame from a time series of vertical-slice images under a breaking wave. The wave is propagating from right to left. The upper edge of the region of highest backscatter (red) provides a good estimate of the surface location, illustrated by the line segment crossing x=0, y=15 m. The red "wedge" extending down and to the right from the highest point on the surface is produced by a cloud of bubbles being actively injected by the breaking wave. Over time this bubble cloud penetrates to between 2 and 3 m depth. A time-delayed correlation technique (PIV) was used to track the mean motion of 2 m squares in the vertical. A set of 16 squares were tracked, centered on the locations indicated by asterisks (*). Arrows indicate estimated vertical velocities of each square at the time of the picture.

This prototype "coherent mode" deployment shows promise, and performance could be improved significantly with a few modest adjustments: (1) A transmitter with much narrower beampattern in the cross-pie direction is needed, to bring that dimension of the sample area into line with the other two spatial dimensions. (2) A position closer to the surface would both reduce the along-wave cell size and increase the permissible sample rate. For example, from 5 m below the surface horizontal resolution at the surface becomes 10 cm, and sample rates up to 150 frames per second are possible. At these rates, coherent phase changes from one ping to the next could be used to refine vertical velocity estimates (actually radial velocity from the sonar) after an initial estimate from feature tracking. The ambiguity velocity would be around 30 cm/s for 200 kHz sound. (3) More receivers would

also help to refine the angular resolution; doubling the number and reducing the range to 5 m would result in 5 cm resolution in both vertical and horizontal. It would appear that much could be learned about the velocity and turbulence structure under breaking waves by this approach.

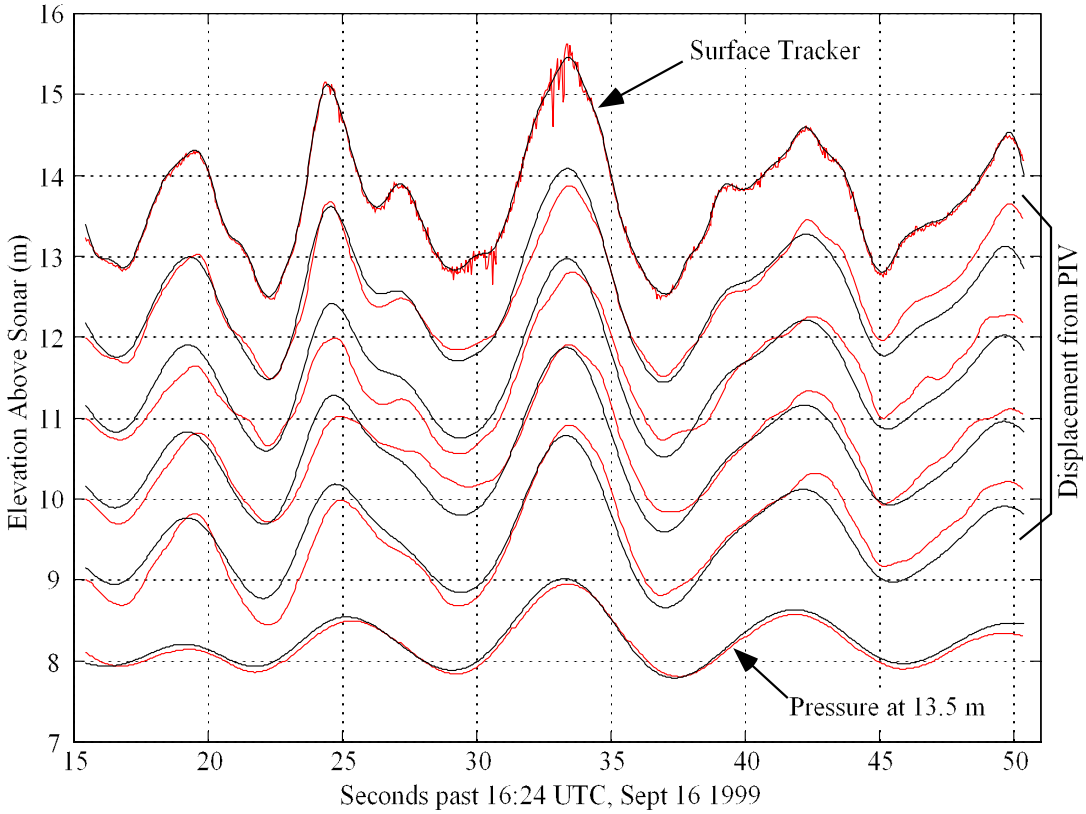

Figure 8. Time-series of (equivalent) vertical displacements at and below the surface. The uppermost trace is from a "surface finder" threshold-based routine. Intense bubble clouds can cause dropouts (jagged red line), so that de-spiking is needed to produce a more reasonable surface estimate (superimposed black line). This trace is characterized by motions near 8 and 5 second periods. Time-delay correlations produce velocity estimates from the heterogeneous intensity fields; these were integrated to synthesize equivalent displacements versus location below the surface ("Displacement from PIV", red lines). The pressure at 13 m mean depth was also recorded (lowest red line). For comparison, an equivalent trace at each depth is computed from the surface track (black lines) using exponential decay versus frequency computed from linear dispersion. Breaking occurs for the second peak, near T = 24.5 s.

References

1. Pinkel R, Smith JA. Repeat-sequence coding for improved precision of Doppler sonar and sodar. *J. Atmos. Oceanic Technol.* 1992; **9**: 149-163.
2. Smith JA, Pinkel R. Improvement of Doppler estimation through repeat sequence coding. In *Oceans '91/Proceedings, October 1-3, 1991, Honolulu, Hawaii, USA/Ocean Technologies and Opportunities in the Pacific for the 90's*, vol. 2. pp. 977-984. Piscataway, N.J.. IEEE; 1991; 977-984.
3. Trevorrow MV, Farmer DM. The use of Barker codes in Doppler sonar measurements. *J. Atmos. Oceanic Technol.* 1992; **9**: 699-704.
4. Crawford CB, Farmer DM. On the spatial distribution of ocean bubbles. *J. Geophys. Res.* 1987; **92**: 8231-8243.
5. Langmuir I. Surface motion of water induced by wind. *Science* 1938; **87**:119-123.
6. Weller R, Dean JP, Marra J, Price J, Francis EA, Boardman DC. Three-dimensional flow in the upper ocean. *Science* 1985; **227**: 1552-1556.
7. Craik ADD, Leibovich S. A rational model for Langmuir circulations. *J. Fluid Mech.* 1976; **73**: 401-426.

8. Craik ADD. The generation of Langmuir circulation by an instability mechanism. *J. Fluid Mech.* 1977; **81**: 209-223.
9. Garrett C. Generation of Langmuir circulations by surface waves– A feedback mechanism. *J. Mar. Res.* 1976; **34**: 117-130.
10. Leibovich S. Convective instability of stably stratified water in the ocean. *J. Fluid Mech.* 1977; **82**: 561-581.
11. Leibovich S. On wave-current interaction theories of Langmuir circulations. *J. Fluid Mech.* 1980; **99**: 715-724.
12. Smith JA. Evolution of Langmuir circulation during a storm. *Journal of Geophysical Research* 1998; **103**: 12,649-612,668.
13. Smith JA. Observations of wind, waves, and the mixed layer: the scaling of surface motion. In *The Wind-Driven Air-Sea Interface* Edited by Banner ML. pp. 231-238. Sydney, Australia. University of New South Wales; 1999. 231-238.
14. Putrevu U, Booker JR, Oltman-Shay J, Pruis MJ. Inverting edge-wave measurements to determine nearshore bathymetry and longshore currents. Part I - Theory and tests. *J. Geophys. Res.* 2000; (submitted).
15. Kennedy AB, Chen Q, Kirby JT, Dalrymple RA. Boussinesq modeling of wave transformation, breaking, end runup. I: 1D. *Journal of Waterway Port Coastal and Ocean Engineering-Asce* 2000; **126**: 39-47.
16. Webb SC, Cox CS. Observations and modeling of seafloor microseisms. *Journal of Geophysical Research* 1986; **91**: 7343-7358.